coatings

MDPI

Article

Micropatterned Polypyrrole/Hydroxyapatite Composite Coatings Promoting Osteoinductive Activity by Electrical Stimulation

Ji Xu [1], Yuan He [1,2,*], Yanan Sun [1], Xiuming Zhang [1], Yunfeng Yi [2], Wei Shi [1,*] and Dongtao Ge [1,*]

[1] The Higher Educational Key Laboratory for Biomedical Engineering of Fujian Province/Research Center of Biomedical Engineering of Xiamen, Xiamen Key Laboratory of Fire Retardant Materials/Fujian Provincial Key Laboratory of Fire Retardant Materials, Department of Biomaterials, College of Materials, Xiamen University, Xiamen 361005, China; 31420191150146@stu.xmu.edu.cn (J.X.); sunyanan@xmu.edu.cn (Y.S.); zhangxiuming@xmu.edu.cn (X.Z.)

[2] Department of Cardiothoracic Surgery, The Affiliated Dongnan Hospital of Xiamen University, Zhangzhou 363005, China; yyfeng.dor1969@163.com

* Correspondence: 20720140153722@stu.xmu.edu.cn (Y.H.); shiwei@xmu.edu.cn (W.S.); gedt@xmu.edu.cn (D.G.)

Abstract: Conductive polypyrrole (PPy) has excellent biocompatibility and structural stability. It is an ideal electroactive biomaterial that can apply exogenous electrical stimulation to promote osteoblast differentiation. However, PPy is a kind of bio-inert material, which does not have osteoinductive capacity. Therefore, we have introduced a kind of bioactive material, hydroxyapatite (HA), to construct PPy/HA composite to enhance bioactivity and osteoinduction. In addition, micron-topological morphology of scattered grid pattern has been designed and introduced to the PPy/HA coatings, which can further enhance the regulation ability of the coatings to the adhesion, proliferation and differentiation of MC3T3-E1 cells. In vitro simulated body fluids (SBFs) immersion test results have demonstrated that the fabricated micropatterned PPy/HA composite coatings perform bioactivity well and can promote the mineral deposition of HA on the surface. Moreover, it can also benefit the proliferation and osteognetic differentiation of MC3T3-E1 cells, when accompanied by external electrical stimulation (ES). In this study, we have successfully constructed electroactive and bioactive coatings, the method of which can potentially be applied to the surface functional modification of traditional bone repair metals.

Keywords: polypyrrole/hydroxyapatite composite; micropatterned; electrical stimulation; MC3T3-E1

Citation: Xu, J.; He, Y.; Sun, Y.; Zhang, X.; Yi, Y.; Shi, W.; Ge, D. Micropatterned Polypyrrole/Hydroxyapatite Composite Coatings Promoting Osteoinductive Activity by Electrical Stimulation. *Coatings* **2022**, *12*, 849. https://doi.org/10.3390/coatings12060849

Academic Editors: Iulian Vasile Antoniac and Shariq Najeeb

Received: 8 May 2022
Accepted: 14 June 2022
Published: 17 June 2022

1. Introduction

The growth and remodeling of bone tissue are accompanied by the generation of endogenous electrical signals [1–4]; therefore, the electrical environment is one of the important microenvironments for bone cells. In fact, external electrical stimulation (ES) has been used in the clinical treatment of bone diseases, such as fractures and osteoporosis [5–7]. Till now, many studies have also confirmed that ES can promote the proliferation and differentiation of osteoblasts [8], so as to promote the formation and regeneration of new bone [9,10]. In addition, the chemical composition and topological morphology of the material surface in contact with cells, and the application of external stimulation signals (electricity, light, magnetism, etc.), have significant impact on the metabolism of cells [11,12]. Therefore, appropriate morphological design, chemical component improvement and external applied stimulation can have important effects on the adhesion, spreading, proliferation and differentiation of cells [13–15]. With the help of some high-precision processing methods, it is possible to design and construct composite structures with different physical and chemical properties and topological morphologies. The micro electro mechanical system (MEMS) integrates many high-precision machining methods, such as lithography, corrosion

and so on [16]. At present, it is widely used to manufacture advanced micro-integrated intelligent packing devices. Application of lithography technology can help to fabricate some patterned structures with micro- or nano-scale graphics. The self-assembled monolayer (SAM) technique could achieve functional modification of materials by adjusting the end groups at both ends of long-chain organic molecules [17].

Conductive polypyrrole (PPy) is an ideal electroactive biomaterial with excellent biocompatibility [18,19], and it can be used as conductive coatings to directly apply ES to cells with electrical response, including osteoblasts, so as to regulate cell behavior and metabolism [20,21]. Many related studies, and our previous works, have also confirmed that PPy, as a kind of conductive coating, can promote the proliferation and differentiation of MECT3-E1 cells with ES [22–26]. However, PPy is a kind of bio-inert material without bioactivity, and cannot induce cell differentiation [27]. Therefore, there is a need to prepare new composite materials to improve the bioactivity of PPy, on the premise of preserving the conductivity [28,29].

Hydroxyapatite (HA, $Ca_{10}(PO_4)_6(OH)_2$) is the main inorganic component of human bone [30,31]. It has excellent biocompatibility, bioactivity, and osteoinductivity [32–36]. Therefore, HA has been applied in clinical bone repair to provide a functional coating, or scaffold, for new bone formation [37–41]. However, the poor mechanical capacity of HA greatly restricts its application. At present, HA is mainly used as the surface modification coating of metal implants [42–44]. Based on the huge differences in physical properties, the interaction is not close [45]. In addition, long-term erosion from immersing in a biologically liquid environment might lead to peeling, dissolution and erosion of HA coatings from the metal surface, thus leading to the failure of the material implantation and tissue repair [46,47].

At present, many researchers are investigating the combination of PPy and HA so as to improve the application of these two materials. Wu et al. chose a pulse electrochemical method and used PPy as a regulator to manufacture a dexamethasone/hydroxyapatite composite coating on a titanium surface, achieving a stable and slow release of HA and dexamethasone, as well as sustained osteoinductivity [26]. Chakraborty et al. synthesized HA-PPy composite coating by pulsed reverse electrochemical deposition, which improved the corrosion protection performance behavior of SS316 [48]. Song et al. fabricated a three-dimensional reduced-graphene oxide/polypyrrole/hydroxyapatite composite scaffold through an electrostatic layer-by-layer assembly strategy, followed by an electrochemical deposition process [49], which had good mechanical properties and good osteogenic performance. However, these studies did not concern themselves with the effect of ES on osteogenesis, and, also, they did not take advantage of two-dimensional topological structuring.

In this work, bioactive and osteoinductive micropatterned PPy/HA composite coatings with micron-scale topological morphology were fabricated, which possess both the electroactivity of PPy and the bioactivity of HA. The electroactive composite coatings were constructed by a two-step method, in which conductive PPy, with micro-scale pattern, was first electrochemically deposited on a micropatterned substrate processed by MEMS technology. Subsequently, HA was further selectively mineral deposited and filled the checkered area with the assistance of SAMs. Characterizations showed that the micropatterned PPy/HA composite coatings maintained good conductivity and electrochemical activity, and could accelerate the deposition of HA on the surface. Moreover, combined with ES, the adhesion, proliferation and differentiation of MC3T3-E1 cells were significantly promoted, and the osteogenesis of MC3T3-E1 cells was accelerated.

2. Materials and Methods

2.1. Materials

Pyrrole (98%) and sodium dodecyl benzene sulfonate (DBS) were obtained from Sinopharm Chemical Reagent Co., Ltd. (Beijing, China). Hexadecanoic acid mercaptan (MDA) was purchased from Alfa Aesar China Chemical Co., Ltd. (Shanghai, China). Other

inorganic salt reagents that were used, such as sodium chloride (NaCl), sodium bicarbonate ($NaHCO_3$) and hydrochloric acid (HCl), were bought from Xilong Chemical Co., Ltd. (Shantou, China).

Pyrrole was purified by distillation under the protection of nitrogen and seal preserved at −20 °C for subsequent use. Other reagents were used directly without further treatment. The water used in all experiments was ultrapure water (18 MΩ).

Monocrystal silicon wafers were cleaned using the RCA standard cleaning method. Then, they were placed in an oxidation diffusion furnace at 950 °C until the thickness of the oxide layer reached 500 nm. Finally, 500 Å Ti and 1000 Å Au were sputtered on the surface of the oxidized silicon wafer. The Au/Ti/Si wafer was used for further experimentation (Figure 1①).

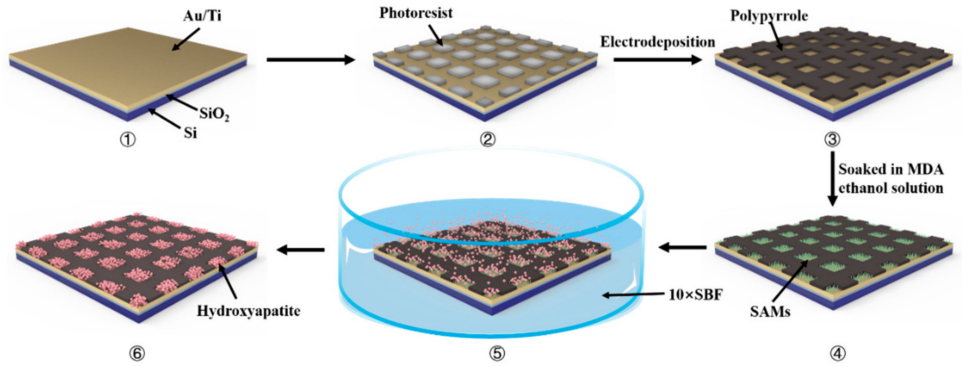

Figure 1. Fabrication process of micropatterned PPy coatings and micropatterned PPy/HA composite coatings. ① The Au/Ti/Si wafer; ② Micropatterned photoresist substrate; ③ The micropatterned PPy; ④ SAM-modified micropatterned PPy coatings; ⑤ The SAM-modified micropatterned PPy coatings soaked in 10× SBF solution; ⑥ The micropatterned PPy/HA composite coatings.

2.2. Fabrication of Micropatterned PPy Coatings

Firstly, micropatterned photoresist substrate (Figure 1②) was prepared by conventional ultraviolet lithography. The photoresist was applied with homogenizer at 2000 rpm/min for 30 s, then put in the oven at 92 °C and baked for 10–12 min. After baking, the photoresist was exposed for 12 s and developed for 90 s. Finally, after cleaning with deionized water and drying with N_2, the micropatterned photoresist was obtained.

Then, PPy was deposited on the prepared micropatterned photoresist substrate by electrochemical polymerization. The process was carried out in a three-electrode system, in which the photoresist Au/Ti/Si wafer was the working electrode, a platinum wire was the counter electrode and a saturated calomel electrode (SCE, INESA Scientific Instrument Co., Ltd. Shanghai, China) was the reference electrode. The 0.1 M pyrrole monomer was dissolved in the electrolyte of aqueous solution (pH = 7.4) containing 0.1 M DBS. The micropatterned PPy coatings were directly electrochemically polymerized on the Au/Ti/Si wafer under a constant current density of 0.1 mA/cm^2 for 1500 s with CHI660D electrochemical workstation (Chenhua Instrument Company, Shanghai, China). Finally, the micropatterned PPy (Figure 1③) was ultrasonically cleaned with acetone and ethanol to remove the photoresist. After washing with ultrapure water, the sample was blow dried with N_2 for further use.

PPy coatings with common morphology were electrochemically deposited on the Au/Ti/Si substrate in the same electrolyte and deposition conditions.

2.3. Fabrication of Micropatterned PPy/HA Composite Coatings

The micropatterned PPy was immersed in 2 mM of fresh MDA ethanol solution for 12–16 h. Based on the interaction between sulfhydryl and Au, MDA molecules would self-assemble in the area uncovered by PPy to form a closely arranged SAM (Figure 1④). Then, the SAM-functionalized micropatterned PPy coatings could be obtained by washing

with ultrapure water and drying with N_2. Finally, the SAM-modified micropatterned PPy coatings were soaked in 10× SBF solution for 2 h (Figure 1⑤). Based on the electrostatic attraction of the active carboxyl groups at the end of the SAMs to Ca^{2+} in solution, Ca^{2+} and PO_4^{3-} ions were selectively aggregated and deposited on the SAMs to induce HA nucleation and growth, so as to obtain micropatterned PPy/HA composite coatings (Figure 1⑥).

2.4. Characterization

The morphologies of micropatterned photoresist on the Au/Ti/Si substrate and micropatterned PPy coatings were observed by metallographic microscopy (L150, Nikon, Germany). The morphologies of micropatterned PPy coatings, micropatterned PPy/HA composite coatings and HA in micropatterned PPy/HA composite coatings were observed by scanning electron microscopy (SEM, LEO1530, Zeiss, Germany) with an accelerating voltage of 20.0 kV. The FTIR spectra of micropatterned PPy and micropatterned PPy/HA composite coatings were analyzed using Fourier transform infrared spectrometer (FTIR, Avatar 360, Nocalet Instrument Corporation, Waltham, MA, USA) with the KBr pellet method. The element composition and crystal structure of deposited HA was further characterized by X-ray energy spectrum (EDS, EDS7426, Oxford Instruments, Oxford, Britain) and X-ray diffraction (XRD, X-pert, Panalytical, Almelo, The Netherlands). The static contact angle of different samples was measured by contact angle meter (JC2000A, Shanghai Zhongchen Digital Technic Apparatus Co., Ltd., Shanghai, China) with water dropped at three different positions of each sample, and each sample was randomly tested in five parallel specimens. The electrochemical activity and stability were characterized by cyclic voltammetry (CV), tested in 0.9% NaCl using a CHI660D electrochemical workstation. The scanning voltage range was −0.9~0.2 V, and the scanning speed was 50 mV/s.

2.5. Bioactivity Assessment

The micropatterned PPy/HA composite coatings were immersed into fresh 1× SBF solution under constant temperature at 36.5 °C, and the 1× SBF solution was replaced every 48 h. The soaked samples were taken out at 2 and 4 days respectively, and the micropatterned PPy/HA composite coatings were washed with deionized water and dried naturally at room temperature, then characterized by SEM, EDS and XRD.

2.6. Cell Culture

The mouse embryonic osteoblast precursor cells (MC3T3-E1) were purchased from the Peking Union Cell Center. MC3T3-E1 cells were cultured in the alpha-modified minimum essential medium (α-MEM, Hyclone, Logan, UT, USA), supplemented with 10% FBS (Gibco, Waltham, MA, USA) and 1% penicillin and streptomycin (Gibco, Waltham, MA, USA) in a humidified 5% CO_2 incubator at 37 °C. The medium was changed every 2 days during the normal subculture of cells.

2.7. Effect of Micropatterned PPy/HA Composite Coatings with ES on MC3T3-E1 Cell Adhesion, Proliferation and Differentiation

The self-made device to exert electrical stimulation was soaked in chromic acid washing solution for more than 12 h, then washed with ultra-pure water and sterilized by high pressure steam sterilization for 20 min. Micropatterned PPy/HA composite coatings, non-patterned PPy, silicon film, copper rods, screws and wires were soaked in 75% alcohol overnight then cleaned with ultra-pure water. Before samples were installed into the electrical stimulation devices, all materials and equipment were irradiated under UV radiation for 1 h.

The sterilized coatings were placed in the self-made electric stimulation devices and the exposed area of coatings in contact with cells was 1.0×0.5 cm^2. Suspension of MC3T3-E1 cells with 2×10^4 cells/mL was seeded into each well and cultured in a cell incubator at 5% CO_2 and 37 °C. The medium was changed every 24 h.

The ES was applied to cells from the day of inoculation with a constant current of 10 μA for 4 h every day for 14 days. The electrical signal was output by an electrochemical workstation using the multi-current steps mode. Each ES chamber (as shown in Figure 2) was connected in a series to the electrochemical workstation through a wire connecting electrode rod.

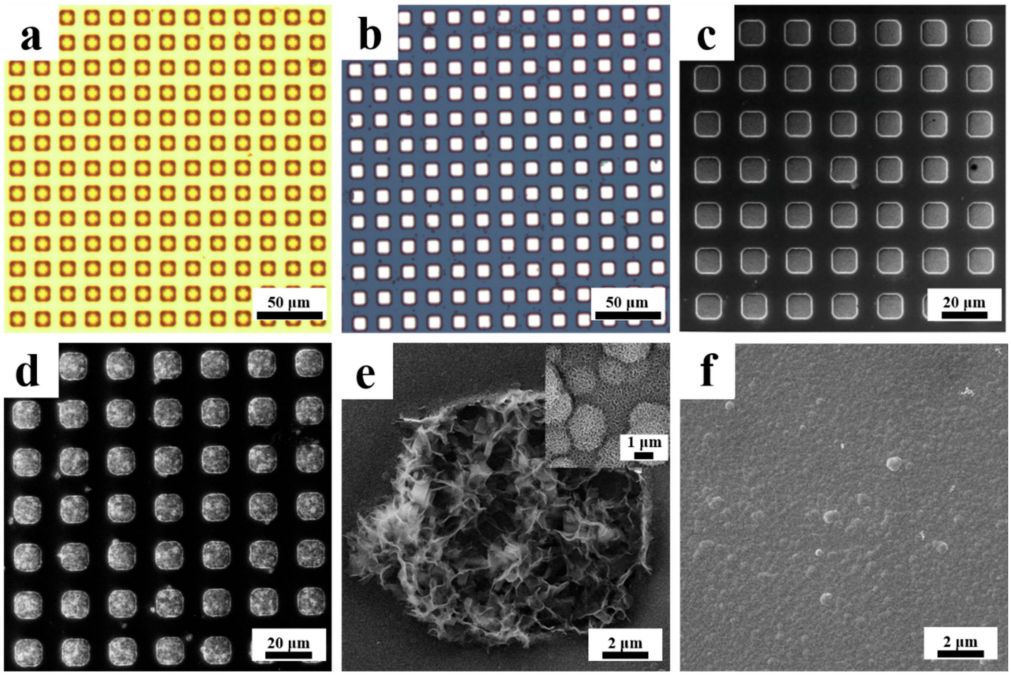

Figure 2. Metallographic microscope image of micropatterned photoresist (**a**) and micropatterned PPy (**b**); SEM image of micropatterned PPy (**c**), micropatterned PPy/HA composite coatings (**d**), local enlarged SEM images of HA (**e**) and PPy (**f**) morphologies in micropatterned PPy/HA composite coatings.

2.7.1. Cell Morphology

The morphology of cells on different coatings was observed by fluorescence microscope (Leica DM2500, Leica Camera, Wetzlar, Germany) and SEM. After MC3T3-E1 cells were cultured for 24 h, cells were stained with 200 μL Calcein-AM staining solution (2 μmol/L) at 37 °C for 15–30 min, then the staining solution was discarded and they were washed with PBS 3 times. Finally, samples were observed by fluorescence microscope.

The cells on different coatings for SEM detection needed to undergo gradient dehydration with ethanol solutions and further dried in a 37 °C oven. Before observation, the sample needed to be sprayed with Au.

2.7.2. MTT Assay

The cell viability of MC3T3-E1 cells growing on different coatings was investigated via MTT assay. MC3T3-E1 cells were cultured with different coatings. At different tested time points (4, 24 and 48 h), the medium was removed and washed twice with PBS, 500 μL of fresh culture medium, without FBS, was mixed with 100 μL MTT working solution (5 mg/mL) and added to each well and co-incubated at 37 °C for 4 h. Finally, the solution was completely removed and 500 μL DMSO was added to fully dissolve the formazan crystals. The testing solution was transferred into a 96-well plate, and the optical density (OD) values at 570 nm were measured by enzyme standardizer (Infinity 200pro, Tecan, Männedorf, Switzerland). This experiment was repeated 4 times and each sample was set in 6 parallel samples.

2.7.3. Determination of the BSA Protein Content, Alkaline Phosphatase Activity (ALP) and Inorganic Calcium Content

The effect of different coatings and ES on MC3T3-E1 cell biosynthesis was evaluated by testing the BSA protein content, ALP activity and inorganic calcium content on the 3rd, 7th and 14th days, respectively. MC3T3-E1 cells in each group were washed with PBS and lysed with 200 μL 0.1% TritonX-100 for 30 min at 4 °C, then the lysate was centrifuged at 4 °C with 3000 rpm/min for 2 min. The supernatant was collected for further detection of protein content and ALP activity. After this, 500 μL HCl (0.1 M) was added to the supernatant, and it was incubated at 4 °C for 4 h to fully dissolve the calcium. Then, the solution was centrifuged at 4 °C with 1000 rpm/min for 2 min. The supernatant was collected for further inorganic calcium content detection.

The total protein content was measured by a commercial BCA protein Assay Kit (Pulley Genetic Technology, Beijing, China) by testing the absorption values at 570 nm. The ALP activity was measured using the commercial ALP Assay Kit (Jiancheng technology Co., Ltd, Nanjing, China) by testing the absorption values at 405 nm. Inorganic calcium content was measured by using a Calcium Assay Kit (Jiancheng technology Co., Ltd, Nanjing, China) by testing the absorption values at 610 nm. These experiments were repeated 3 times. In each experiment, 4 parallel samples of each coating were set, and the absorption values were measured with enzyme standardizer.

3. Results and Discussion

3.1. Preparation and Characterization of Micropatterned PPy/HA Composite Coatings

The process of micropatterned PPy/HA composite coating preparation is shown in Figure 1. In brief, evenly distributed square micropattern was first fabricated on an/a Au/Ti/Si substrate by photolithography. Metallographic microscope images showed that the micropatterned photoresist was distributed in a regular lattice on the Au/Ti/Si substrate and consisted of squares with side length and spacing of 10 μm (Figure 2a). Subsequently, the photoresist micropatterned Au/Ti/Si substrate was used as the template, and PPy was selectively electrochemically polymerized on the conductive areas uncovered by photoresist. After the photoresist was removed, it could be seen that the continuous grid PPy coatings with smooth and flat surface were successfully deposited and the boundary of the pattern was clear (Figure 2b,c). Next, based on the strong interaction between the sulfhydryl group and Au, functional 16-mercaptohexadecanoic acid (MDA) SAMs were constructed on the exposed Au regions. Meanwhile, the carboxyl group at the exposed end of the MDA SAMs could attract Ca^{2+} by electrostatic interaction, and then adsorbed Ca^{2+} continued to attract anions, including phosphate and hydroxyl, thus inducing the nucleation and mineralization growth of HA. Under the environment of high concentration SBF (10×), SAMs could more quickly induce the rapid and localized growth of HA in the SAMs' covered areas. By soaking in 10× SBF for only 2 h, HA could highly selectively fill the grid pattern without invading other PPy covered areas (Figure 2d), and the growing HA showed a typical chrysanthemum-like crystal morphology (Figure 2e). Thus, we obtained micropatterned PPy/HA composite coatings. The PPy with ordinary morphology coatings, as the control group, had the same micro-morphology as the PPy part in micropatterned PPy/HA composite coatings, showing a typical cauliflower shape (Figure 2f).

The chemical structures of the PPy and HA parts in PPy/HA composites were characterized by FTIR, respectively. From the FTIR spectra of PPy and HA, it could be seen that characteristic peaks of PPy appeared at 3346 cm^{-1}, corresponding to N-H stretching vibration and 1465 cm^{-1} ascribing to C=N/N-H stretching vibrations in the pyrrole ring. In addition, peaks at 1090, 604, 563 and 436 cm^{-1} were basically consistent with the characteristic peaks of PO_4^{3-} in HA. Moreover, the peaks at 1456 and 1405 cm^{-1}, attributed to CO_3^{2-}, indicated $CaCO_3$ existed in the mineralized HA (Figure 3a). The EDS was carried out to semi-quantitatively analyze elements in the HA part, and Ca, P, O, C, etc. elements were detected. Among them, the Ca/P ratio was about 1.1–1.4 at different regions, which was between the theoretical Ca/P ratio of HA (1.67) and $CaHPO_4 \cdot 2H_2O$ (DCPD, 1.0) [50]

(Figure 3b). Therefore, it could be inferred that a variety of minerals composed of apatite, dominated by HA, were deposited in 10× SBF. Therefore, it was speculated that the deposition obtained from 10× SBF was a mixture mineral, including HA and other apatites. At the same time, the crystal diffraction peak analysis of the deposited mineral was obtained by XRD and also confirmed that there were at least two types of crystals, including DCPD and HA (Figure 3c). The contact angle tests showed that the micropatterned PPy/HA composite coatings had good surface hydrophilicity (Figure 3d).

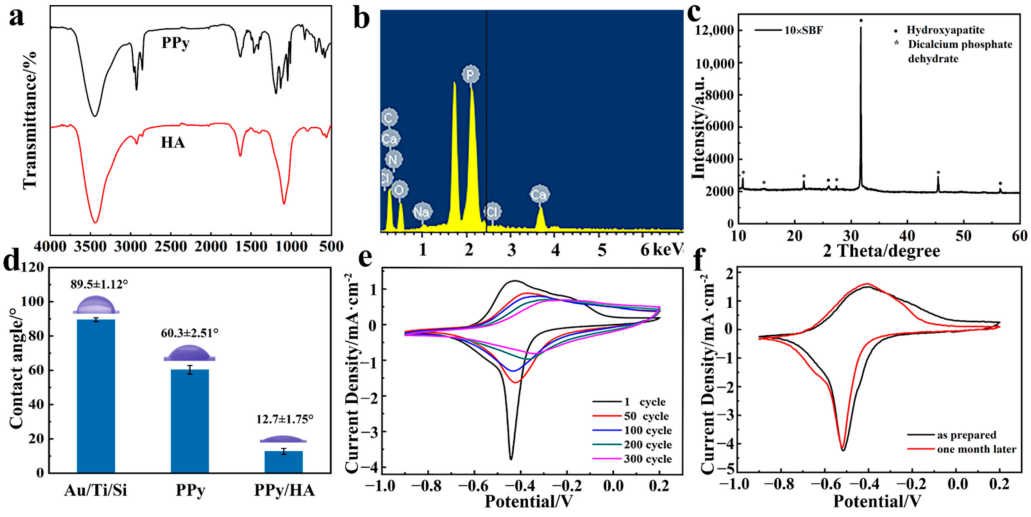

Figure 3. (**a**) FITR spectra of micropatterned PPy and HA in micropatterned PPy/HA composite coatings; (**b**) EDS spectrum of micropatterned PPy/HA composite coatings; (**c**) XRD spectrum of micropatterned PPy/HA composite coatings; (**d**) The water contact angle of different material substrates; (**e**) Cyclic voltammogramms of micropatterned PPy in 0.9% NaCl solution with different cycle turns at the scan rate of 50 mV/s; (**f**) Long-term electroactive stability of micropatterned PPy at the scan rate of 50 mV/s.

On the PPy/HA composite coatings, the micropatterned PPy still existed as a continuous structure, which ensured the conductivity of the composite coatings. The conductivity of micropatterned PPy coatings was about 10 S/cm, which made the feasibility of subsequent ES on cells valid. In addition, considering the composite coatings needed to be immersed in medium with applied electrical signals for a long time, in subsequent experiments we further evaluated the bonding and electrical stabilities of the micropatterned PPy/HA composite coatings. It was noted that the PPy could uphold a relatively stable redox property after multiple cycles of a CV scanning test (Figure 3e). Furthermore, the electrochemical activity of the micropatterned PPy/HA composite coatings did not change significantly even after soaking in solution for 1 month, which also demonstrated that the micropatterned PPy coatings could maintain stable adhesion with the substrate under the applied ES for a long time (Figure 3f).

3.2. Bioactivity Assessment of Micropatterned PPy/HA Composite Coatings

An ideal bone repair material should not only have excellent biocompatibility, but also possess biological activity. Bioactive materials can quickly exchange ions with human body fluid in the body, and form HA layers similar to the composition of natural bone tissue on the surface through a series of reactions, which is beneficial to the forming of a stable chemical interaction with bone to further induce tissue regeneration. Hence, HA was introduced into the micropatterned PPy coatings to enhance the bioactivity. The bioactivity of micropatterned PPy/HA composite coatings to promote HA deposition in vitro was evaluated with simulated body fluid (1× SBF).

Immersing micropatterned PPy/HA composite coatings in SBF (×1) with standard concentration, it was found that the HA part acted as nucleation sites to promote further

mineralized deposition of HA. From the SEM images, it could be seen that newly formed HA covered the original HA region and continued to epitaxially grow after soaking in 1× SBF for only 2 d. Till the 4th d, HA almost enclosed the whole substrate and formed a new layer of HA (Figure 4a,b). However, no HA crystals were observed on pure PPy coatings under the same conditions (Figure 4c). These results indicated that the PPy/HA composite coatings had excellent biological activity and could quickly induce the mineral deposition of HA.

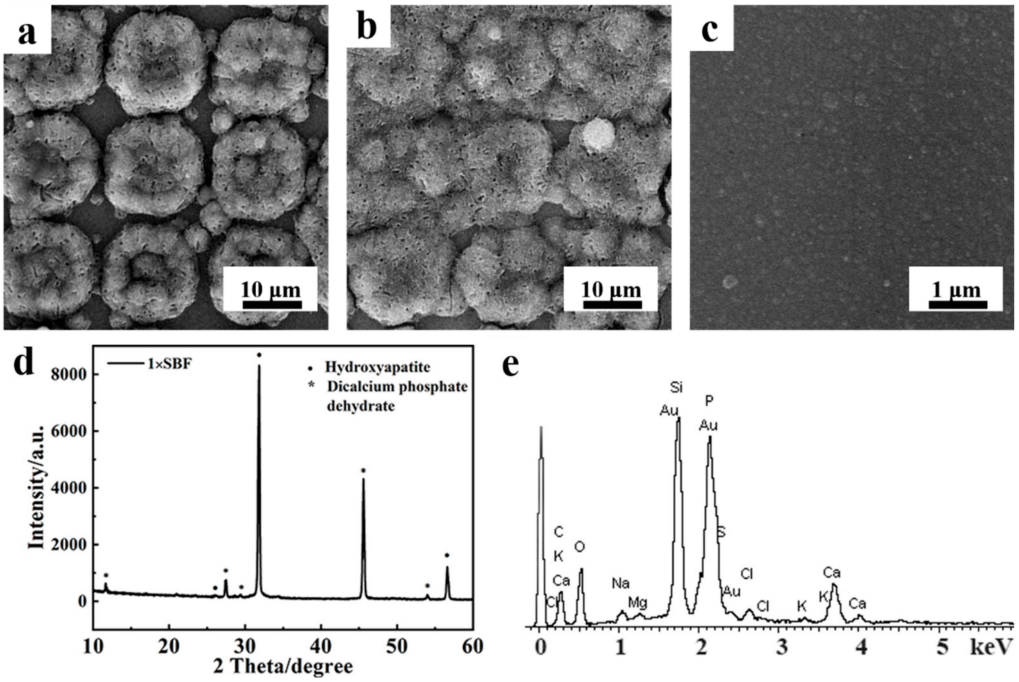

Figure 4. SEM images of micropatterned PPy/HA composite coatings soaked in 1× SBF for 2 d (**a**) and 4 d (**b**); (**c**) SEM image of unpatterned PPy soaked in 1× SBF for 4 d; (**d**) XRD spectrum of micropatterned PPy/HA composite coatings soaked in 1× SBF for 4 d; (**e**) EDS spectrum of micropatterned PPy/HA composite coatings soaked in 1× SBF for 4 d.

The EDS and XRD tests of the newly deposited HA layer displayed that the Ca/P ratio of the induced formed HA was about 1.70, which was very close to that of natural HA (Figure 4d,e). Combined with the results of XRD (Figure 4e), these results both demonstrated that the bioactive composite coatings could induce the deposition of HA with similar chemical structure to natural HA.

3.3. Effect of Micropatterned PPy/HA Composite Coatings with ES on Cell Activity

To investigate the positive effect of micropatterned PPy/HA composite coatings and the synergistic effect with ES on adhesion, spreading and proliferation of MC3T3-E1 cells, the cell activity and morphology of the contact between MC3T3-E1 cells with different materials were assessed. The attachment and spreading of cells on the substrates are the prerequisites for subsequent osteogenic differentiation. The interaction between the cell and substrate is intuitively reflected in the spreading morphology of cells. From the fluorescent images, it could be directly observed that there were significantly more MC3T3-E1 cells when the cells were co-cultured with different coating materials for 24 h on two different substrates with ES, than were the cases with the other two groups without ES. Moreover, whether ES was applied or not, cells preferred to grow on the micropatterned PPy/HA composite coatings, compared to the PPy coatings with ordinary morphology (Figure 5a–d). In total, micropatterned PPy/HA composite coatings together with ES had a synergistic effect on MC3T3-E1 cells. SEM images more intuitively showed the adhesion and spreading behavior of cells on different substrates (Figure 5e–h). Actually,

it was noted that MC3T3-E1cells presented a slender spindle shape on the surface of un-patterned PPy coatings, while a more stretched polygon shape, with many cell bumps, were observed on the micropatterned PPy/HA composite coatings. This indicated that MC3T3-E1 cells had a more thorough spreading shape and larger spreading area on the micropatterned PPy/HA composite coatings surface than on the ordinary PPy coatings, and that the micropatterned PPy/HA composite coatings surface was conductive for cells to contact each other and transmit relevant signals. Furthermore, MC3T3-E1 cells growing on micropatterned PPy/HA composite coatings with ES stretched out more pseudopodia and cell synapses, which suggested that cells had closer interaction and tighter adhesion with the substrate.

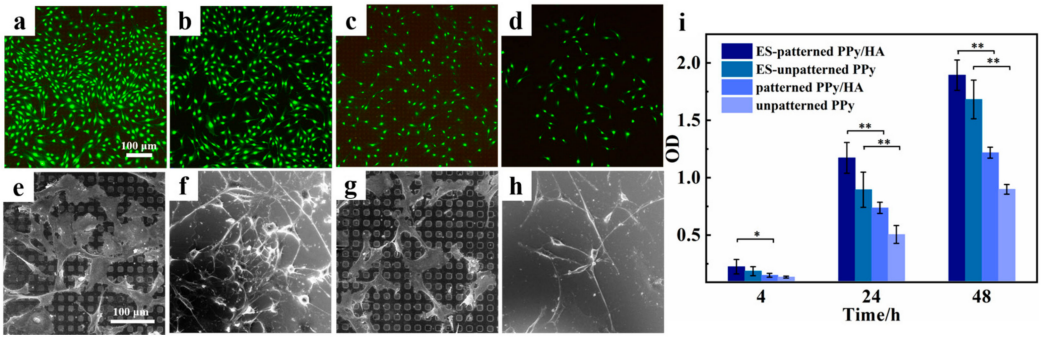

Figure 5. (**a**–**d**) Fluorescence images of MC3T3-E1 cells cultured on different materials for 24 h; (**a**) Micropatterned PPy/HA composite coatings with ES; (**b**) Unpatterned PPy with ES; (**c**) Micropatterned PPy/HA composite coatings without ES; (**d**) Unpatterned PPy without ES; (**e**,**f**) SEM images of MC3T3-E1 cells cultured on different materials for 24 h; (**e**) Micropatterned PPy/HA composite coatings with ES; (**f**) Unpatterned PPy with ES; (**g**) Micropatterned PPy/HA composite coatings without ES; (**h**) Unpatterned PPy without ES; (**i**) Cell adhesion and proliferation curves of MC3T3-E1 cells on different materials. * $p < 0.05$, ** $p < 0.01$.

The proliferation of MC3T3-E1 cells cultured on different material surfaces and with or without ES was evaluated by MTT assay. During the first 4–6 h after cells were inoculated on different substrate materials, the main behavior of cells was to adhere to the surface of the materials. As shown in Figure 5i, the adhesion of MC3T3-E1 cells on different materials displayed significant disparity after 4 h, when more cells adhered to the two kinds of coatings with ES than to those without ES, and micropatterned coatings accompanied with ES had the most positive effect on promoting cell adhesion. Cell proliferation continued to be detected on different materials, and it was noted that the proliferation rate of ME3T3-E1 cells with ES was obviously faster than without ES. Moreover, the advantage of promoting cell proliferation by coatings with micropatterned morphology appeared, and the synergistic effect of micropatterned PPy/HA composite coatings together with ES resulted in the most efficient performance and the promotion of proliferation of MC3T3-E1 cells.

3.4. Effect of Micropatterned PPy/HA Composite Coatings with ES on Cell Functional Characteristics

When osteoblasts adhere to the surface of the material and proliferate rapidly, they initiate the synthesis of related proteins [51]. Therefore, the assay of the total cellular protein content could reflect the cell survival and proliferation. Based on the total protein content of MC3T3-E1 cells grown on different materials (Figure 6a), it could be seen that the total protein content increased with time in all groups, indicating that all groups of materials could promote the secretion and synthesis of proteins. Protein synthesis in cells with high proliferative activity was more abundant and metabolically vigorous, which could disperse, spread and multiply on the material surface in a short period of time. The protein content of cells on the micropatterned PPy/HA composite coatings was higher than that on the un-patterned PPy, which indicated that the modification of HA and micropatterning can

promote cell adhesion, spreading and proliferation, thus, further promoting the increase of total cellular protein content. The cellular protein content on all materials of the ES groups was significantly higher than that of the non-ES groups, and the discrepancy was greatest at 14 d. This indicated that the cellular growth state was exuberant with ES, resulting in a significant increase in cellular protein synthesis. The highest protein content was found in the group wherein cells grew on micropatterned PPy/HA composite coatings with ES, demonstrating that MC3T3-E1 cells under this culture condition had more vigorous metabolic and proliferative activities.

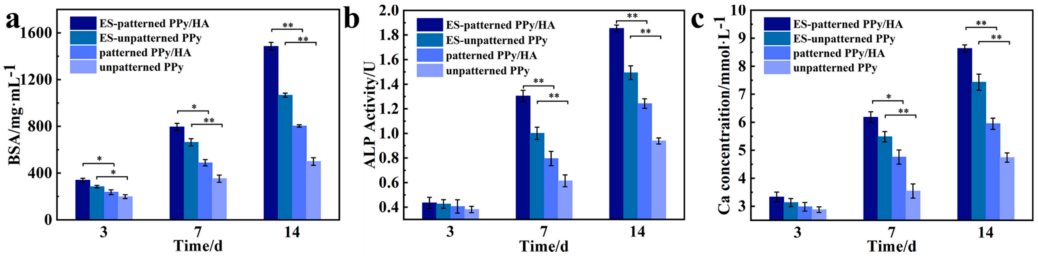

Figure 6. (**a**) BSA protein content of MC3T3-E1 cells cultured on different materials; (**b**) The ALP activities of MC3T3-E1 cells cultured on different materials; (**c**) The inorganic calcium content of MC3T3-E1 cells cultured on different materials. * $p < 0.05$, ** $p < 0.01$.

ALP is an early symbol of osteoblast differentiation and functional maturation. ALP could enhance the local concentration of phosphorus in vivo to promote the nucleation and mineralization of HA in bone tissue, and thus start the process of ECM mineralization. By detecting the changes of ALP activity, we could intuitively show the differentiation, maturity and bone mineralization ability of MC3T3-E1 cells. The results of the ALP activity assay of MC3T3-E1 cells on different coatings are shown in Figure 6b. After culturing for 3 d, the ALP activity of MC3T3-E1 cells on all coatings was low and did not show significant differences. This indicated that the cells were in the proliferation stage at this time, and the cells had not started the differentiation process. With the extension of time, the ALP activity in all groups increased significantly, and the differences between different groups were gradually obvious. Till the 7th d, the ALP activity of the ES groups was significantly higher than that of the non-ES groups and the ALP activity of the cells on the micropatterned PPy/HA composite coatings with ES was the highest, which was almost 2.2-times higher than that of the PPy with ordinary morphology, without ES (the control group). The ALP activity in the ES or micropatterned factors alone groups only increased 1.6 and 1.3 folds, respectively. At the 14th d, since no effective induction conditions were applied, the ALP activity in the control group still had no obvious change, but the ALP activity of MC3T3-E1 cells in the other three groups continued to increase. Among them, the ALP activity of MC3T3-E1 cells on the micropatterned PPy/HA composite coatings together with ES still maintained the advantage over the other groups, being almost twice as high as the control group. The above results further confirmed that micropatterned PPy/HA composite coatings with ES have synergetic effects on the functional differentiation of cells and can significantly promote the mineralization and osteogenesis of MC3T3-E1 cells.

Their calcification ability is an important biological characteristic of osteoblasts. The inorganic calcium content of the cells was measured to investigate the calcification ability in osteoblasts. As seen in Figure 6c, the calcium content in all groups was very close and at a relatively low concentration level at the 3rd d. This was because cellular calcium ion deposition occurs mainly during the matrix calcification phase after the increase of ALP activity, so the cellular calcium content of the micropatterned PPy/HA composite coatings with ES group started to be significantly higher than the rest of groups until the 7th d, and increased almost 1.8-fold more than that in control group. When cells were cultured until the 14th d, most MC3T3-E1 cells had matured and entered the matrix calcification phase, which led to the calcium content constant increasing significantly. The calcium content of the cells on the micropatterned PPy/HA composite coatings was significantly higher

than that on other groups. The result was consistent with the results of the BSA protein content and ALP activity assay experiments, and demonstrated again that micropatterned PPy/HA composite coatings with ES can promote the cellular matrix mineralization of osteoblasts, thus promoting new osteogenesis.

4. Conclusions

In summary, we designed and fabricated bioactive micropatterned PPy/HA composite coatings. The composite coatings had both the advantages of excellent conductivity and electrochemical activity from PPy and good biological activity from HA, and further constructed topological microstructures with scattered square morphology by MEMS and SAM technology. In vitro experimentation demonstrated that micropatterned PPy/HA composite coatings had excellent mineralization inducing activity, which could induce and shorten the mineral deposition time of HA in SBF solution. Moreover, the results of cell experiments further verified that the micropatterned PPy/HA composite coatings performed excellent bioactivity and osteoinductivity. When combined with externally applied ES, the composite coatings could promote the adhesion, proliferation and osteogenic differentiation of MC3T3-E1 cells growing on them. Therefore, the micropatterned PPy/HA composite coatings are functional coatings with excellent biocompatibility and bioactivity, and can be regarded as an ideal strategy to improve the surface bioactivity and osteoinductivity of bone transplantation and to repair metal materials.

Author Contributions: Methodology, J.X., W.S. and D.G. Investigation, J.X. and Y.H. Writing—original draft preparation, J.X. and Y.H. Writing—review and editing, Y.S., X.Z., Y.Y., W.S. and D.G. All authors have read and agreed to the published version of the manuscript.

Funding: This work was supported by the National Natural Science Foundation of China (31271009, 81271689, 31870986, 22172132), the Program for New Century Excellent Talents in University, the Natural Science Foundation of Fujian Province (2020J01036), and the Foundation of Xiamen Science and Technology Bureau (3502Z20209206).

Institutional Review Board Statement: Not applicable.

Informed Consent Statement: Not applicable.

Data Availability Statement: Data available on request from the authors.

Acknowledgments: We acknowledge the analysis and testing center of Xiamen University.

Conflicts of Interest: The authors declare no conflict of interest.

References

1. Isaacson, B.M.; Bloebaum, R.D. Bone bioelectricity: What have we learned in the past 160 years? *J. Biomed. Mater. Res. Part A* **2010**, *95*, 1270–1279. [CrossRef] [PubMed]
2. Huang, Y.; Jing, W.; Li, Y.; Cai, Q.; Yang, X. Composites made of polyorganophosphazene and carbon nanotube up-regulating osteogenic activity of BMSCs under electrical stimulation. *Colloids Surf. B* **2021**, *204*, 111785. [CrossRef] [PubMed]
3. Sahm, F.; Ziebart, J.; Jonitz-Heincke, A.; Hansmann, D.; Dauben, T.; Bader, R. Alternating electric fields modify the function of human osteoblasts growing on and in the surroundings of titanium electrodes. *Int. J. Mol. Sci.* **2020**, *21*, 6944. [CrossRef] [PubMed]
4. Zheng, T.; Huang, Y.; Zhang, X.; Cai, Q.; Deng, X.; Yang, X. Mimicking the electrophysiological microenvironment of bone tissue using electroactive materials to promote its regeneration. *J. Mater. Chem. B* **2020**, *8*, 10221–10256. [CrossRef] [PubMed]
5. Leppik, L.; Oliveira, K.M.; Bhavsar, M.B.; Barker, J.H. Electrical stimulation in bone tissue engineering treatments. *Eur. J. Trauma Emerg. Surg.* **2020**, *46*, 231–244. [CrossRef]
6. Eischen-Loges, M.; Oliveira, K.M.; Bhaysar, M.B.; Barker, J.H.; Leppik, L. Pretreating mesenchymal stem cells with electrical stimulation causes sustained long-lasting pro-osteogenic effects. *PeerJ* **2018**, *6*, 4959. [CrossRef]
7. Bhavsar, M.B.; Han, Z.; DeCoster, T.; Leppik, L.; Oliveira, K.M.; Barker, J.H. Electrical stimulation-based bone fracture treatment, if it works so well why do not more surgeons use it? *Eur. J. Trauma Emerg. Surg.* **2020**, *46*, 245–264. [CrossRef]
8. Samadian, H.; Mobasheri, H.; Hasanpour, S.; Ai, J.; Azamie, M.; Faridi-Majidi, R. Electro-conductive carbon nanofibers as the promising interfacial biomaterials for bone tissue engineering. *J. Mol. Liq.* **2020**, *298*, 112021–112028. [CrossRef]

9. Li, P.; Zhang, S.; Li, K.; Wang, J.; Liu, M.; Gu, X.; Fan, Y. The promoting effect on pre-osteoblast growth under electrical and magnetic double stimulation based on PEDOT/Fe_3O_4/PLGA magnetic-conductive bi-functional scaffolds. *J. Mater. Chem. B* **2018**, *6*, 4952–4962. [CrossRef]
10. Das, R.; Curry, E.J.; Le, T.T.; Awale, G.; Liu, Y.; Li, S.; Contreras, J.; Bednarz, C.; Millender, J.; Xin, X.; et al. Biodegradable nanofiber bone-tissue scaffold as remotely-controlled and self-powering electrical stimulator. *Nano Energy* **2020**, *76*, 105028–105039. [CrossRef]
11. Thrivikraman, G.; Lee, P.S.; Hess, R.; Haenchen, V.; Basu, B.; Schamweber, D. Interplay of substrate conductivity, cellular microenvironment, and pulsatile electrical stimulation toward osteogenesis of human mesenchymal stem cells in vitro. *ACS Appl. Mater. Interfaces* **2015**, *7*, 23015–23028. [CrossRef] [PubMed]
12. Yuan, Z.; Wan, Z.; Wei, P.; Lu, X.; Mao, J.; Cai, Q.; Zhang, X.; Yang, X. Dual-controlled release of icariin/Mg^{2+} from biodegradable microspheres and their synergistic upregulation effect on bone regeneration. *Adv. Healthc. Mater.* **2020**, *9*, 2000211–2000224. [CrossRef] [PubMed]
13. Luo, Y.; Shen, H.; Fang, Y.; Cao, Y.; Huang, J.; Zhang, M.; Dai, J.; Shi, X.; Zhang, Z. Enhanced proliferation and osteogenic differentiation of mesenchymal stem cells on graphene oxide-incorporated electrospun poly(lactic-co-glycolic acid) nanofibrous mats. *ACS Appl. Mater. Interfaces* **2015**, *7*, 6331–6339. [CrossRef] [PubMed]
14. Ji, H.; Sun, H.; Qu, X. Antibacterial applications of graphene-based nanomaterials: Recent achievements and challenges. *Adv. Drug Deliv. Rev.* **2016**, *105*, 176–189. [CrossRef] [PubMed]
15. Zhu, J.; Qi, Z.; Zheng, C.; Xue, P.; Fu, C.; Pan, S.; Yang, X. Enhanced Cell Proliferation and Osteogenesis Differentiation through a Combined Treatment of Poly-L-Lysine-Coated PLGA/Graphene Oxide Hybrid Fiber Matrices and Electrical Stimulation. *J. Nanomater.* **2020**, *2020*, 5892506. [CrossRef]
16. Golvari, P.; Kuebler, S.M. Fabrication of functional microdevices in SU-8 by multi-photon lithography. *Micromachines* **2021**, *12*, 472. [CrossRef]
17. Love, J.C.; Estroff, L.A.; Kriebel, J.K.; Nuzzo, R.G.; Whitesides, G.M. Self-assembled monolayers of thiolates on metals as a form of nanotechnology. *Chem. Rev.* **2005**, *105*, 1103–1169. [CrossRef]
18. Zare, E.N.; Agarwal, T.; Zarepour, A.; Pinelli, F.; Zarrabi, A.; Rossi, F.; Ashrafizadeh, M.; Maleki, A.; Shahbazi, M.A.; Maiti, T.K.; et al. Electroconductive multi-functional polypyrrole composites for biomedical applications. *Appl. Mater. Today* **2021**, *24*, 101117–101152. [CrossRef]
19. Balint, R.; Cassidy, N.J.; Cartmell, S.H. Conductive polymers: Towards a smart biomaterial for tissue engineering. *Acta Biomater.* **2014**, *10*, 2341–2353. [CrossRef]
20. Liang, Y.; Goh, J. Polypyrrole-incorporated conducting constructs for tissue engineering applications: A review. *Bioelectricity* **2020**, *2*, 101–119. [CrossRef]
21. Wu, M.; Zhang, F.; Zhang, Y.; Zhang, H.; Zhao, Y.; Xu, X.; Qin, M.; Ding, C.; Li, J. Electrically facilitated mineralization of osteoblasts and polypyrrole micro-bowl coatings for promotion of the osteogenic activity. *Colloid Interface Sci. Commun.* **2021**, *43*, 100450–100459. [CrossRef]
22. He, Y.; Wang, S.; Mu, J.; Dai, L.; Zhang, Z.; Sun, Y.; Shi, W.; Ge, D. Synthesis of polypyrrole nanowires with positive effect on MC3T3-E1 cell functions through electrical stimulation. *Mater. Sci. Eng. C* **2017**, *71*, 43–50. [CrossRef] [PubMed]
23. Hu, W.W.; Hsu, Y.T.; Cheng, Y.C.; Li, C.; Ruaan, R.C.; Chien, C.C.; Chung, C.A.; Tsao, C.W. Electrical stimulation to promote osteogenesis using conductive polypyrrole films. *Mater. Sci. Eng. C-Mater.* **2014**, *37*, 28–36. [CrossRef] [PubMed]
24. Zhou, Z.; Yu, P.; Zhou, L.; Tu, L.; Fan, L.; Zhang, F.; Dai, C.; Liu, Y.; Ning, C.; Du, J.; et al. Polypyrrole nanocones and dynamic piezoelectric stimulation-induced stem cell osteogenic differentiation. *ACS Biomater. Sci. Eng.* **2019**, *5*, 4386–4392. [CrossRef]
25. He, Y.; Dai, L.; Zhang, X.; Sun, Y.; Shi, W.; Ge, D. The Bioactive Polypyrrole/polydopamine nanowire coating with enhanced osteogenic differentiation ability with electrical stimulation. *Coatings* **2020**, *10*, 1189. [CrossRef]
26. Liao, J.; Chen, W.; Yang, M.; Zhou, J.; Wang, Z.; Zhou, Y.; Ning, C.; Yuan, H. Conducting photopolymers on orthopeadic implants having a switch of priority between promoting osteogenic and antibacterial activity. *Mater. Horiz.* **2018**, *5*, 545–552. [CrossRef]
27. Zhou, T.; Yan, L.; Xie, C.; Li, P.; Jiang, L.; Fang, J.; Zhao, C.; Ren, F.; Wang, K.; Wang, Y.; et al. A mussel-inspired persistent ROS-scavenging, electroactive, and osteoinductive scaffold based on electrochemical-driven in situ nanoassembly. *Small* **2019**, *15*, 1805440–1805453. [CrossRef]
28. Wu, H.; Gao, Y.; Xiao, L.; Wei, Q.; Zhang, N.; Su, Z.; Ma, C.; Ye, T.; Wang, Y. Polypyrrole doping-regulated construction of dexamethasone/hydroxyapatite composite coating on titanium surface for sustained osteoinduction. *Mater. Des.* **2021**, *202*, 109571–109582. [CrossRef]
29. Zhang, Q.; Qiao, Y.; Zhu, J.; Li, Y.; Li, C.; Lin, J.; Li, X.; Han, H.; Mao, J.; Wang, F.; et al. Electroactive and antibacterial surgical sutures based on chitosan-gelatin/tannic acid/polypyrrole composite coating. *Compos. B Eng.* **2021**, *223*, 109140–109152. [CrossRef]
30. Christy, P.N.; Basha, S.K.; Kumari, V.S.; Bashir, A.K.; Maaza, M.; Kaviyarasu, K.; Arasu, M.V.; Al-Dhabi, N.A.; Ignacimuthu, S. Biopolymeric nanocomposite scaffolds for bone tissue engineering applications—A review. *J. Drug Deliv. Sci. Technol.* **2020**, *55*, 101452. [CrossRef]
31. LeGeros, R.Z. Properties of osteoconductive biomaterials: Calcium phosphates. *Clin. Orthop. Relat. Res.* **2002**, *395*, 81–98. [CrossRef] [PubMed]

32. Shin, K.; Acri, T.; Geary, S.; Salem, A.K. Biomimetic mineralization of biomaterials using simulated body fluids for bone tissue engineering and regenerative medicine. *Tissue Eng. Part A* **2017**, *23*, 1169–1180. [CrossRef] [PubMed]
33. Roohani-Esfahani, S.I.; No, Y.J.; Lu, Z.; Ng, P.Y.; Chen, Y.; Shi, J.; Pavlos, N.J.; Zreiqat, H. A bioceramic with enhanced osteogenic properties to regulate the function of osteoblastic and osteocalastic cells for bone tissue regeneration. *Biomed. Mater.* **2016**, *11*, 035018. [CrossRef] [PubMed]
34. Sharifianjazi, F.; Esmaeilkhanian, A.; Moradi, M.; Pakseresht, A.; Asl, M.S.; Karimi-Maleh, H.; Jang, H.W.; Shokouhimehr, M.; Varma, R.S. Biocompatibility and mechanical properties of pigeon bone waste extracted natural nano-hydroxyapatite for bone tissue engineering. *Mater. Sci. Eng. B Adv.* **2021**, *264*, 114950. [CrossRef]
35. Wu, S.C.; Hsu, H.C.; Liu, M.Y.; Ho, W.F. Characterization of nanosized hydroxyapatite prepared by an aqueous precipitation method using eggshells and mulberry leaf extract. *J. Korean Ceram. Soc.* **2021**, *58*, 116–122. [CrossRef]
36. Fedotov, A.Y.; Kotyakov, A.A.; Smirnov, I.V.; Zobkov, Y.V.; Baranov, O.V.; Egorov, A.A.; Teterina, A.Y.; Rad'kova, E.A.; Tyut'kova, Y.B.; Barinov, S.M.; et al. Coatings of low-temperature calcium phosphates on hydroxyapatite ceramic. *Inorg. Mater. Appl. Res.* **2021**, *12*, 940–945. [CrossRef]
37. Shi, P.; Liu, M.; Fan, F.; Yu, C.; Lu, W.; Du, M. Characterization of natural hydroxyapatite originated from fish bone and its biocompatibility with osteoblasts. *Mater. Sci. Eng. C* **2018**, *90*, 706–712. [CrossRef]
38. Ramesh, N.; Moratti, S.C.; Dias, G.J. Hydroxyapatite-polymer biocomposites for bone regeneration: A review of current trends. *J. Biomed.* **2018**, *106*, 2046–2057. [CrossRef]
39. Nezafati, N.; Farokhi, M.; Heydari, M.; Hesaraki, S.; Nasab, N.A. In vitro bioactivity and cytocompatablity of an injectable calcium phosphate cement/silanated gelatin microsphere composite bone cement. *Compos. B Eng.* **2019**, *175*, 107146. [CrossRef]
40. Song, Y.; Wu, H.; Gao, Y.; Li, J.; Lin, K.; Liu, B.; Lei, X.; Cheng, P.; Zhang, S.; Wang, Y.; et al. Zinc silicate/nano-hydroxyapatite/collagen scaffolds promote angiogenesis and bone regeneration via the p38 MAPK pathway in activated monocytes. *ACS Appl. Mater. Interfaces* **2020**, *12*, 16058–16075. [CrossRef]
41. Ievlev, V.M.; Kostyuchenko, A.V.; Kochlar, G.S.; Putlyaev, V.I. Structure and nanohardness of compact hydroxyapatite-based ceramics. *Inorg. Mater.* **2019**, *55*, 1054–1060. [CrossRef]
42. Cao, Y.; Shi, T.; Jiao, C.; Liang, H.; Chen, R.; Tian, Z.; Zou, A.; Yang, Y.; Wei, Z.; Wang, C.; et al. Fabrication and properties of zirconia/hydroxyapatite composite scaffold based on digital light processing. *Ceram. Int.* **2020**, *46*, 2300–2308. [CrossRef]
43. Arifin, A.; Sulong, A.B.; Muhamad, N.; Syarif, J.; Ramli, M.I. Material processing of hydroxyapatite and titanium alloy (HA/Ti) composite as implant materials using powder metallurgy: A review. *Mater. Des.* **2014**, *55*, 165–175. [CrossRef]
44. Chueva, T.R.; Gamurar, N.V.; Kalita, V.I.; Komlev, D.I.; Radyuk, A.A.; Komlev, V.S.; Teterina, A.Y.; Shamray, V.F.; Mikhailova, A.B. Influence of titanium substrate temperature on phase structure of a plasma hydroxyapatite coating. *Inorg. Mater. Appl. Res.* **2022**, *13*, 386–392. [CrossRef]
45. Paital, S.R.; Dahotre, N.B. Calcium phosphate coatings for bio-implant applications: Materials, performance factors, and methodologies. *Mater. Sci. Eng. R Rep.* **2009**, *66*, 1–70. [CrossRef]
46. Gross, K.A.; Berndt, C.C. Thermal processing of hydroxyapatite for coating production. *J. Biomed. Mater. Res.* **1998**, *39*, 580–587. [CrossRef]
47. Wei, M.; Ruys, A.J.; Milthorpe, B.K.; Sorrell, C.C.; Evans, J.H. Electrophoretic deposition of hydroxyapatite coatings on metal substrates: A nanoparticulate dual-coating approach. *J. Sol-Gel Sci. Technol.* **2001**, *21*, 39–48. [CrossRef]
48. Chakraborty, R.; Seesala, V.S.; Manna, J.S.; Saha, P.; Dhara, S. Synthesis, characterization and cytocompatibility assessment of hydroxyapatite-polypyrrole composite coating synthesized through pulsed reverse electrochemical deposition. *Mater. Sci. Eng. C* **2019**, *94*, 597–607. [CrossRef]
49. Song, F.; Jie, W.; Zhang, T.; Li, W.; Jiang, Y.; Wan, L.; Liu, W.; Li, X.; Liu, B. Room-temperature fabrication of a three-dimensional reduced-graphene oxide/polypyrrole/hydroxyapatite composite scaffold for bone tissue engineering. *RSC Adv.* **2016**, *6*, 92804–92812. [CrossRef]
50. Wang, H.B.; Lee, J.K.; Moursi, A.; Lannutti, J.J. Ca/P ratio effects on the degradation of hydroxyapatite in vitro. *J. Biomed. Mater. Res. Part A* **2003**, *67*, 599–608. [CrossRef]
51. Yang, Y.Z.; Cavin, R.; Ong, J.L. Protein adsorption on titanium surfaces and their effect on osteoblast attachment. *J. Biomed. Mater. Res. Part A* **2003**, *67*, 344–349. [CrossRef] [PubMed]